Perovskites

Deutsche Ausgabe: DOI: 10.1002/ange.201607397
Internationale Ausgabe: DOI: 10.1002/anie.201607397

Benign-by-Design Solventless Mechanochemical Synthesis of Three-, Two-, and One-Dimensional Hybrid Perovskites

Alexander D. Jodlowski, Alfonso Yépez, Rafael Luque, Luis Camacho, and Gustavo de Miguel**

Abstract: *Organic–inorganic hybrid perovskites have attracted significant attention owing to their extraordinary optoelectronic properties with applications in the fields of solar energy, lighting, photodetectors, and lasers. The rational design of these hybrid materials is a key factor in the optimization of their performance in perovskite-based devices. Herein, a mechanochemical approach is proposed as a highly efficient, simple, and reproducible method for the preparation of four types of hybrid perovskites, which were obtained in large amounts as polycrystalline powders with high purity and excellent optoelectronics properties. Two archetypal three-dimensional (3D) perovskites ($MAPbI_3$ and $FAPbI_3$) were synthesized, together with a bidimensional (2D) perovskite (Gua_2PbI_4) and a "double-chain" one-dimensional (1D) perovskite ($GuaPbI_3$), whose structure was elucidated by X-ray diffraction.*

Three-dimensional (3D) organic–inorganic hybrid perovskites recently emerged as a breakthrough in the field of photovoltaics owing to their potential to enable power-conversion efficiencies (ca. 20%) in perovskite-based devices that are comparable to those reported for commercial silicon-based solar cells.[1] This change of paradigm in photovoltaics prompted a renaissance of interest in the wider family of hybrid perovskites, including two-dimensional (2D), one-dimensional (1D), and zero-dimensional (0D) materials, with improved flexibility in the type of organic cations that can be employed.[2] The rediscovery of these new types of hybrid materials opened up a multitude of optoelectronics applications that remained unexplored for many years, including light-emitting diodes,[3] photodetectors,[4] and lasing.[5] However, the excellent optoelectronic properties of these materials and, more importantly, their impact on the performance of perovskite-based devices are highly sensitive to the adopted synthetic strategy. In general, the preparation of particular device architectures incorporating high-quality perovskite crystals is required for most applications. Traditional synthetic methods to prepare hybrid perovskites include 1) precipitation from solution and 2) gas-phase deposition.[6] In the solution-based method, stoichiometric mixtures of metal halides and organic ammonium halide precursors are normally dissolved in dimethylformamide (DMF) or dimethyl sulfoxide (DMSO). For the preparation of single perovskite crystals at the micrometer scale, the solvent is allowed to slowly evaporate at room temperature or under mild heating. However, the solution containing the precursors needs to be spread homogeneously over a substrate by different methods (spin coating, spray coating, screen printing, or dip coating) for the preparation of thin films and/or for particular applications.[7] The deposition can be carried out in a single-step process or through a two-step process, in which the metal halide is first deposited on the substrate, followed by the subsequent incorporation of the organic cation into the film to form the perovskite. In the vapor-phase method, the precursors are generally coevaporated in a vacuum deposition chamber onto a substrate by the use of two separate sources to form uniform and controlled-thickness films.[8] Despite the remarkable advances in the development of simple and inexpensive methods to fabricate 3D hybrid perovskites, significant efforts are ongoing in the design of new strategies that allow the synthesis of high-quality crystals.

Mechanochemistry has emerged as an attractive alternative synthetic process featuring remarkable simplicity, swiftness, and reproducibility in line with unprecedented green credentials (e.g. solventless solid-state synthesis) for the design of a wide range of nanomaterials, including supported nanoparticles and MOFs.[9] The combination of the mechanical energy generated under ball-milling conditions and the inherent chemical modification of structures/surfaces make this methodology extremely promising for nanomaterials design, particularly for alternative greener perovskite syntheses.

We disclose herein a novel and efficient mechanochemical approach for the design of polycrystalline hybrid perovskites. The precursors used in this study, PbI_2 and methylammonium (MAI), formamidinium (FAI), or guanidinium iodide (GuaI), were mixed in a 1:1 molar ratio inside a ball mill under an ambient atmosphere to produce large amounts of polycrystalline powders. One of the main advantages of the proposed protocol is the solventless nature of the synthetic process for perovskite formation. Further advantages are the swiftness, simplicity, and reproducibility of the method as well as its significant potential for extension to the design of various structures. In this way, two 3D hybrid perovskites ($MAPbI_3$ and $FAPbI_3$), a 2D perovskite containing Gua, and a "double-

[*] A. D. Jodlowski, Prof. L. Camacho, Prof. G. de Miguel
Institute of Fine Chemistry and Nanochemistry
Department of Physical Chemistry and Applied Thermodynamics
University of Cordoba, Campus Universitario de Rabanales
Edificio Marie Curie, 14014 Córdoba (Spain)
E-mail: gmiguel@uco.es
Dr. A. Yépez, Prof. R. Luque
Departamento de Química Orgánica, Universidad de Córdoba
Edificio Marie Curie, Ctra Nnal IVa Km 396, 14014 Córdoba (Spain)
E-mail: q62alsor@uco.es

Supporting information and the ORCID identification number(s) for the author(s) of this article can be found under http://dx.doi.org/10.1002/anie.201607397.

chain" 1D perovskite with $GuaPbI_3$ stoichiometry were synthesized. In particular, the structure of 1D $GuaPbI_3$ perovskite was elucidated for the first time owing to the high purity of the polycrystalline powder.[10] The different powders were characterized comprehensively by X-ray diffraction, diffuse reflectance spectroscopy, X-ray photoelectron spectroscopy, thermogravimetric analysis, differential scanning calorimetry, and scanning electron microscopy.

Figure 1 shows a photograph of the black powder synthesized with MAI (left), the light-yellow powder synthesized with FAI (center left), and the intense-yellow powder synthesized with GuaI (center). We annealed all powders up to approximately 170 °C in an oven and then cooled them down to room temperature to explore potential phase transitions or further chemical reactions that could potentially take place in the materials. The powder prepared with FAI turned black at approximately 150 °C and remained black upon cooling to 30 °C (Figure 1, center right). The black color of the powders prepared with MAI and FAI agrees well with those reported for the well-known 3D hybrid perovskites $MAPbI_3$ and α-$FAPbI_3$ prepared by other synthetic protocols.[11] Annealing gave a pale-yellow powder for material prepared with GuaI, and this color also remained unchanged after cooling to room temperature (Figure 1, right).

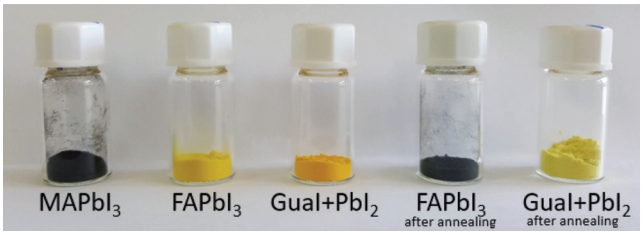

Figure 1. Photograph of the different as-prepared powders synthesized by ball milling. The black powder containing FAI (center-right vial) and the pale-yellow powder with GuaI (right vial) were obtained by heating the corresponding as-prepared powders at 170 °C, followed by cooling to room temperature.

To assess the existence of phase transitions and the stability of the as-prepared powders, we conducted thermogravimetric analysis (TGA) and differential scanning calorimetry (DSC) for each sample (see Figure S1 in the Supporting Information). The TGA curves of powders prepared with MAI and FAI showed no significant weight loss up to 250–300 °C. In both cases, this behavior supports the good stability of the 3D hybrid perovskite particles, which started to degrade at 250 °C (usually associated with the loss of HI).[12] A closer examination of the TGA curves pointed to a slight drop in the signal (0.05–0.1 %) around 55 and 130 °C. Well-defined endothermic peaks could be observed around 60 and 135 °C in the DSC curves for $MAPbI_3$ and $FAPbI_3$, respectively. These temperatures are in good agreement with reported phase transitions from tetragonal to cubic symmetry in $MAPbI_3$ and from a non-perovskite phase (δ-phase) to trigonal symmetry (α-phase) in $FAPbI_3$.[11] Furthermore, the DSC curves also revealed additional endothermic peaks at 115 and 138 °C for $MAPbI_3$ and 87 and 173 °C for $FAPbI_3$. These signals could be assigned to the elimination of water upon heating, since the same perovskites prepared by solvent-assisted methods also revealed a minor weight loss at approximately 100 °C associated with physisorbed water as well as another signal drop at 180 °C attributed to more strongly bound water.[13] No weight loss was observed in the studied temperature range (up to 200 °C) for powders prepared with GuaI before annealing (see Figure S1 C), with the presence of an endothermic peak at 134 °C as observed by DSC analysis. Similarly, no weight loss was detected in the same sample after annealing (Figure S1 D), with the DSC analysis showing an endothermic peak shifted to 160 °C, as reported for a perovskite with $GuaPbI_3$ stochiometry.[14]

We subsequently characterized the crystalline powders obtained from the mechanosynthesis process by X-ray diffraction (XRD) studies to investigate the nature and purity of the perovskite materials. The experimental XRD pattern for the powder prepared with MAI (Figure 2 A)

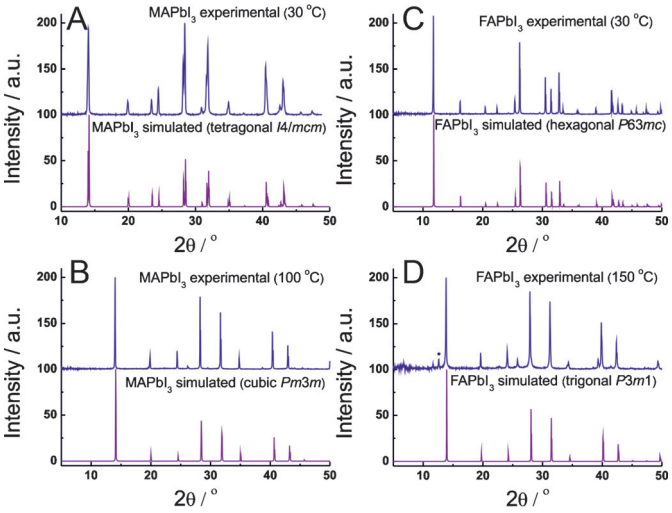

Figure 2. Blue lines: Experimental XRD patterns of the powders synthesized with MAI at 30 (A) and 100 °C (B), and with FAI at 30 (C) and 150 °C (D). Purple lines: Simulated XRD patterns for the 3D hybrid perovskites $MAPbI_3$, in the tetragonal (A) and cubic phase (B), and $FAPbI_3$, with hexagonal (C) and trigonal symmetry (D). The star in (D) indicates the reflection peak of PbI_2.

revealed a tetragonal structure of the 3D hybrid $MAPbI_3$ perovskite upon comparison with the previously reported simulated structure pattern (*I4/mcm* space group).[11] The lattice parameters derived from our crystallographic analysis (see Figure S2 A) are $a = b = 8.879(3)$ Å and $c = 12.663(4)$ Å, highly consistent with those previously reported.[11] Clearly, no diffraction peaks of the precursors (typically present as characteristic diffraction peaks at 12.8° for PbI_2 and 20° for MAI) are visible in the experimental diffractogram. These findings demonstrate the high yields of the mechanochemical synthesis of $MAPbI_3$ with the absence of crystalline impurities. To investigate the phase transitions of $MAPbI_3$, we conducted variable-temperature powder XRD analysis of the as-prepared powders. The XRD patterns (30–100 °C) showed an abrupt disappearance of reflections at 23.4 and 30.9° in the

55–60 °C temperature range (see Figure S3), thus matching the DSC results. This behavior was previously ascribed definitively to a change in the crystallographic phase from tetragonal to cubic symmetry in $MAPbI_3$.[11] No changes were evident in the XRD patterns upon increasing the temperature up to 100 °C, thus confirming the high stability of the cubic phase in the studied temperature range. Figure 2B displays the experimental (at 100 °C) and simulated (*Pm*3*m* space group) XRD patterns for the cubic $MAPbI_3$ structure, with an excellent match between the two patterns. From a Pawley data fit, we obtained a lattice parameter of $a = b = c =$ 6.3430(9) Å (see Figure S2B).

Figure 2C shows XRD powder patterns for samples prepared with FAI and PbI_2 at room temperature as well as the simulated pattern for the δ-phase of the $FAPbI_3$ structure.[11] Excellent agreement was observed between the two patterns, with no residual reflection peaks from any other concurrent structure, thus demonstrating the presence of a pure phase obtained under ball milling. The absence of impurities in this material can contribute to its rapid implementation in optoelectronics. A Pawley fit of the experimental XRD pattern (see Figure S2C) allowed us to obtain the lattice parameters of the unit cell: $a = b = 8.6838$-(7) Å and $c = 7.9306(7)$ Å. δ-$FAPbI_3$ is a layered crystal structure with hexagonal symmetry (*P*63*mc* space group) and no straightforward applications in photovoltaics owing to its limited absorption in the visible range.[11] However, at higher temperature, δ-$FAPbI_3$ is transformed into the α-$FAPbI_3$ phase with excellent photophysical properties for electronic applications. The δ-$FAPbI_3$ powder was heated up to 160 °C, and XRD measurements were gradually recorded to determine phase changes. Figure 3A shows XRD patterns of $FAPbI_3$ from 30 to 160 °C and again at 30 °C after cooling of the sample. There was a sharp change in the diffraction pattern between 140 and 150 °C, consistent with that reported previously (ca. 140 °C) for the corresponding phase transformation.[11] The α-$FAPbI_3$ structure possesses trigonal symmetry (*P*3*m*1 space group) with lattice parameters of $a = b = 9.049(2)$ Å and $c = 11.069(2)$ Å, as obtained by crystallographic analysis of the XRD pattern at 160 °C (see Figure S2D). Even though the majority of the diffraction peaks were indexed to the α-$FAPbI_3$ structure at higher temperatures, a minor peak at 12.6° corresponding to PbI_2 was detected in the XRD pattern. This result has also been reported for $FAPbI_3$ structures prepared by solution methods.[11] The XRD patterns at 160 °C and 30 °C after cooling are identical, thus pointing to an irreversible or slow α-to-δ-$FAPbI_3$ phase transformation in this polycrystalline powder material.

Figure 3B shows the XRD pattern for the as-prepared powder with GuaI (blue line), with no signal of unreacted GuaI and a moderate peak at 12.7° indicating the presence of some PbI_2. Interestingly, most of the remaining peaks in the XRD pattern can be reasonably assigned to a previously reported bidimensional (2D) hybrid perovskite (Gua_2PbI_4 stoichiometry) with orthorhombic symmetry.[15] Unlike the 3D hybrid perovskites synthesized with MAI and FAI, this 2D hybrid perovskite consists of corrugated sheets of the $(PbI_4)_n^{2-}$ polyanion, with the Gua cations enclosed in voids

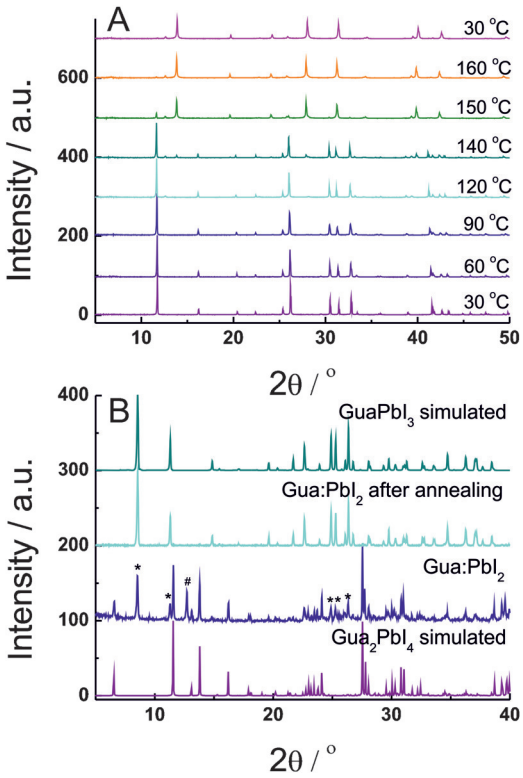

Figure 3. A) XRD patterns at different temperatures of the powder synthesized with FAI. B) XRD patterns of the as-prepared powder with GuaI:PbI_2 at 30 °C (blue line) and after the annealing process at 160 °C (light-blue line). The simulated XRD patterns of Gua_2PbI_4 and $GuaPbI_3$ are shown for comparison. The hash sign (#) in (B) indicates the reflection peak of PbI_2. The stars (B) indicate reflection peaks from the $GuaPbI_3$ structure.

and channels between the neighboring sheets.[15] In the proposed mechanochemical synthesis, the 2D perovskite is not produced quantitatively, since some PbI_2 remained unreacted. Indeed, to induce the full reactivity of PbI_2 to obtain a pure phase, we carried out the annealing process at 170 °C for 300 min and thus obtained the previously described pale-yellow powder. XRD patterns revealed the complete disappearance of the PbI_2 reflection peak at 12.7°. In principle, a reaction may take place within the 2D hybrid perovskite during annealing, as PbI_2 is thermally stable up to 300 °C. The loss of all reflection peaks assigned to the 2D hybrid perovskite upon heating proved the previous assumption. Simultaneously, new reflection peaks appeared in the final XRD pattern, which seemed to correspond to the product of the reaction $PbI_2 + Gua_2PbI_4$. The powder obtained from the annealing process turned orange when heated to 170 °C. This behavior has been reported previously for the formation of $GuaPbI_3$ perovskite phases, although no further information concerning its structure was provided to date.[14]

We performed crystallographic analysis of the final XRD pattern after annealing to enable the complete assignment of all reflection peaks within the orthorhombic symmetry (*Pna*21 space group; Table 1). The elucidated structure corresponds to a 1D hybrid perovskite comprising

Table 1: Crystal data and structure refinement for $GuaPbI_3$ at 303 K.

Chemical formula	$PbI_3N_3CH_6$
Wavelength	1.540562 Å
Crystallographic system	orthorhombic
Space group	*Pna*21
Unit-cell dimensions	$a = 11.990(7)$ Å $b = 20.880(9)$ Å $c = 4.476(2)$ Å
Unit-cell volume	1120.68 Å^3
Z	4
Density	3.8406 g cm^{-3}
Absorption coefficient	23.259 mm^{-1}
2θ range for data collection	2–39.993°
Step size	0.016°
Time per step	288 s
Refinement method	Rietveld
R_{wp}	0.056
R_{wb}	0.056
R_p	0.099
CMACS	0.73%
DOF	23

a "double chain" of inorganic PbI_3^- separated by Gua cations stabilizing the negative charges through electrostatic interactions (Figure 4). Similar inorganic crystal structures were formed previously by the use of various organic cations, including MA and H_2O or DMF, benzidine, and 4,4′-methylenedianilinium.[16] The particular feature defining this crystal structure is the small value for one of the lattice parameters of approximately 4.5 Å. The elucidation of the crystal structure of the perovskite containing the Gua cation ($GuaPbI_3$ stochiometry) could be particularly valuable in the field of photovoltaics owing to the increasing interest in using this symmetric cation, which could remove the hysteresis of the *I–V* curves.[17]

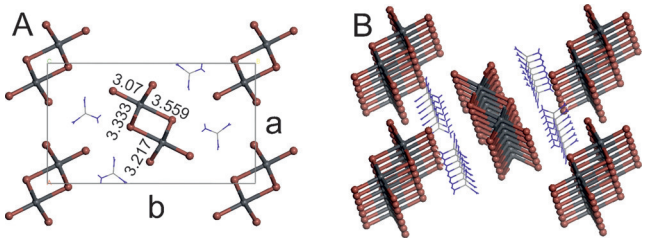

Figure 4. Crystal structure of $GuaPbI_3$. A) Unit cell viewed down the *c*-axis, showing the different Pb—I bond distances. B) Overview of the "double-chain" assembly in the $GuaPbI_3$ 1D hybrid perovskite.

We also performed theoretical calculations for insight into the band structure of 1D $GuaPbI_3$ (for full details, see the Supporting Information). The main contribution to the top valence band is from the I 5p state, with minor contributions from Pb 2s, Pb 5p and N 2p (see Figure S5). In the bottom conduction bands, the main component is Pb 6p, with minor contributions from I 6s and I 6p. These results indicate that I 5p electrons can be photoexcited to Pb 6p empty states (see Figure S5), in analogy with previous reports for $MAPbI_3$.[18] However, there is an additional contribution of the N 2p state at the valence band, unlike the behavior in $MAPbI_3$. The theoretical band-gap energy obtained from this calculation is 2.1 eV. The calculated band structure of 1D $GuaPbI_3$ shows a minimum band gap at the Γ symmetry point (see Figure S6). Both the top valence band and the bottom conduction band are broad, thus indicating the nonlocalized character of the states.

X-ray photoelectron spectroscopy (XPS) measurements were also conducted and confirmed the stoichiometry of the crystal structures as determined by XRD (for full details, see the Supporting Information). In particular, XPS measurements revealed the absence of metallic Pb in our mechanochemically synthesized perovskite materials, whereas metallic Pb is found in materials prepared by solvent-assisted methods.[19] Since the presence of metallic Pb is associated with iodide deficiencies, we conclude that our perovskite crystals lack these types of defects. The lack of these defects could have a beneficial impact on optoelectronic applications of these materials. We used scanning electron microscopy (SEM) to image the morphology and sizes of the synthesized materials and found particles with a distribution of sizes in the range of 10–200 μm for $MAPbI_3$ and $FAPbI_3$. The large size of the synthesized crystals originates from a lower concentration of surface states and bulk defects than in perovskite crystals prepared by solvent-assisted processes.[20] Extensive details of both investigations with additional discussion have been included in the Supporting Information.

The absorption capacity of each perovskite powder was investigated by diffuse reflectance UV/Vis spectroscopy. The optical absorption coefficient (α) can be calculated according to the Kubelka–Munk equation, $F(R) = \alpha = (1\text{-}R)^2/2R$, in which R is the reflectance of each sample.[21] Figure 5 A shows the four absorption spectra for $MAPbI_3$ (black line), $FAPbI_3$ (green line), $GuaPbI_3$ (orange line), and Gua_2PbI_4 (brown line). The last spectrum resembles that of PbI_2 (the unreacted precursor of this synthesis), thus preventing the identification of the absorption features of the 2D perovskite. In the other perovskite materials, the absorption spectra are characterized by a broad and featureless absorption band typical of hybrid perovskites, with the absorption band edge shifted to the low-energy region when going from $GuaPbI_3$ (ca. 500 nm) to $MAPbI_3$ (ca. 800 nm) and $FAPbI_3$ (ca. 850 nm). The large blue shift of the absorption band in $GuaPbI_3$ as compared to that of $MAPbI_3$ and $FAPbI_3$ is associated with the disruption of the 3D network of PbI_6^- octahedra owing to the bulky Gua cations in the 1D "double-chain" structure of $GuaPbI_3$. In particular for the $MAPbI_3$ and $FAPbI_3$ materials, the extrapolation of the absorption of direct transitions at the edge gives a band gap (E_g) of 1.51 and 1.41 eV, respectively (Figure 5 B).[11] These values are in good agreement with those reported for single crystals or polycrystalline samples with large crystal sizes (> 500 nm), thus strongly supporting the SEM results.[22] The small values of E_g in our $MAPbI_3$ and $FAPbI_3$ powders as compared to those found in thin films are a clear indication of the high quality of the crystals with decreased localized defect states.[11c] Regarding the band gap of $GuaPbI_3$, the extrapolation of the sharp absorption edge points to a band gap of 2.25 eV, which is fairly similar to the theoretical value and an experimental value

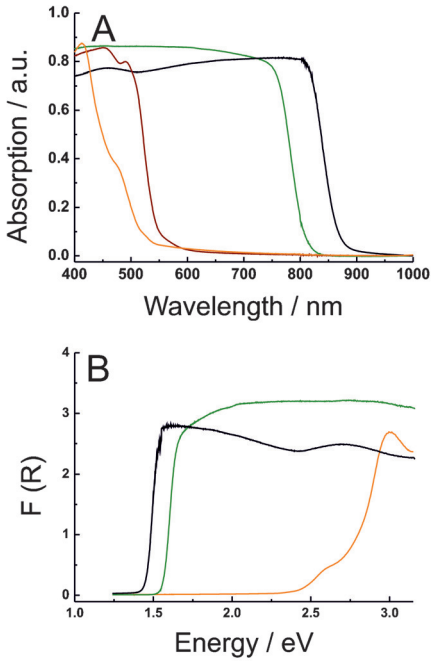

Figure 5. A) UV/Vis absorption spectra obtained in diffuse reflectance mode for the four synthesized powders: $MAPbI_3$ (green line), $FAPbI_3$ (black line), Gua_2PbI_4 (brown line), and $GuaPbI_3$ (orange line). B) Kubelka–Munk spectra of $MAPbI_3$ (green line), $FAPbI_3$ (black line), and $GuaPbI_3$ (orange line).

(2.16 eV) reported for stripelike crystallites of $GuaPbI_3$ synthesized by cooling down an aqueous solution containing the precursors.[23]

We conducted steady-state and time-resolved fluorescence measurements for all perovskite powders to investigate the optoeletronic properties of these materials. Clear emission spectra were observed for each powder with maxima (λ_{max}) in the near-infrared region at 770 and 795 nm for $MAPbI_3$ and $FAPbI_3$ and at around 525 nm for both guanidinium-based perovskites, $GuaPbI_3$ and Gua_2PbI_4 (see Figure S10). The λ_{max} values for both 3D perovskites are in close agreement with those reported for single crystals, whereby an increasing size of the crystals involves a redshift of the λ_{max} value.[11c] The fluorescence lifetimes obtained from a biexponential fit of the data were 4.5 and 37.1 ns for $MAPbI_3$ and 3.0 and 25.2 ns for $FAPbI_3$ (see Table S4). The fluorescence lifetimes are considerably longer than those reported for small grains but not as long as those reported for single crystals.[24] The relatively long fluorescence lifetimes are also a strong indication of a reduced concentration of surface and bulk defects.[24]

To evaluate the potential incorporation of designed perovskites in layered structures of optoelectronic devices, we prepared homogeneous thin films by spin coating on quartz substrates from DMF solutions. The fluorescence lifetimes measured for thin films (see Figure S11 for the steady-state absorption and emission spectra for all synthesized perovskites) were even longer than those observed for the powders (see Table S4). These results indicate that our 1D, 2D, and 3D hybrid perovskites synthesized by ball milling could potentially be used in the fabrication of optoelectronic devices.

In conclusion, the proposed mechanochemical synthesis offers a simple, efficient, and highly reproducible approach for the design of advanced hybrid perovskites, including 3D, 2D, and 1D materials. This solventless synthetic method is expected to pave the way for the further discovery and design of novel perovskite materials with useful properties, as currently under investigation by our research group. Additionally, the facile and cost-efficient preparation of large quantities of the perovskite materials (ca. 5–10 g per batch) remarkably simplifies their use in unexplored strategies for optoelectronics applications.

Acknowledgements

G.d.M. thanks the Ministry of Economy and Competitiveness for a "Ramón y Cajal" contract (RYC-2013-12772). G.d.M. and L.C. acknowledge the Ministry of Economy and Competitiveness for financial support (CTQ2014-56422-P). We are grateful to Prof. Carlos Pérez for his help with the XRD measurements and Prof. Vidal Barrón for his assistance with diffuse reflectance spectroscopy.

Keywords: ball milling · hybrid materials · optoelectronic properties · perovskite phases · powder X-ray diffraction

How to cite: *Angew. Chem. Int. Ed.* **2016**, *55*, 14972–14977
Angew. Chem. **2016**, *128*, 15196–15201

[1] a) M. M. Lee, J. Teuscher, T. Miyasaka, T. N. Murakami, H. J. Snaith, *Science* **2012**, *338*, 643–647; b) J. Burschka, N. Pellet, S. J. Moon, R. Humphry-Baker, P. Gao, M. K. Nazeeruddin, M. Gratzel, *Nature* **2013**, *499*, 316–319; c) H. Zhou, Q. Chen, G. Li, S. Luo, T.-b. Song, H.-S. Duan, Z. Hong, J. You, Y. Liu, Y. Yang, *Science* **2014**, *345*, 542–546; d) W. S. Yang, J. H. Noh, N. J. Jeon, Y. C. Kim, S. Ryu, J. Seo, S. I. Seok, *Science* **2015**, *348*, 1234–1237.

[2] a) B. Sarapov, D. Mitzi, *Chem. Rev.* **2016**, *116*, 4558–4596; b) K. Meg, S. Gao, L. Wu, G. Wang, X. Liu, G. Chen, Z. Liu, G. Chen, *Nano Lett.* **2016**, *16*, 4166–4173.

[3] a) M. Yuan, L. N. Quan, R. Comin, G. Walters, R. Sabatini, O. Voznyy, S. Hoogland, Y. Zhao, E. M. Beauregard, P. Kanjanaboos, Z. Lu, D. H. Kim, E. H. Sargent, *Nat. Nanotechnol.* **2016**, *11*, 872–877; b) S. D. Stranks, H. J. Snaith, *Nat. Nanotechnol.* **2015**, *10*, 391–402; c) H. Cho, S.-H. Jeong, M.-H. Park, Y.-H. Kim, C. Wolf, C.-L. Lee, J. H. Heo, A. Sadhanala, N. Myoung, S. Yoo, S. H. Im, R. H. Friend, T.-W. Lee, *Science* **2015**, *350*, 1222–1225; d) Y. Ling, Z. Yuan, Y. Tian, X. Wang, J. C. Wang, Y. Xin, K. Hanson, B. Ma, H. Gao, *Adv. Mater.* **2016**, *28*, 305–311.

[4] a) Y. Fang, Q. Dong, Y. Shao, Y. Yuan, J. Huang, *Nat. Photonics* **2015**, *9*, 679–686; b) B. R. Sutherland, A. K. Johnston, A. H. Ip, J. Xu, V. Adinolfi, P. Kanjanaboos, E. H. Sargent, *ACS Photonics* **2015**, *2*, 1117–1123; c) L. Dou, Y. Yang, J. You, Z. Hong, W.-H. Chang, G. Li, Y. Yang, *Nat. Commun.* **2014**, *5*, 5404.

[5] a) H. Zhu, Y. Fu, F. Meng, X. Wu, Z. Gong, Q. Ding, M. V. Gustafsson, M. T. Trinh, S. Jin, X.-Y. Zhu, *Nat. Mater.* **2015**, *14*, 636–642; b) S. A. Veldhuis, P. P. Boix, N. Yantara, M. Li, T. C. Sum, N. Mathews, S. G. Mhaisalkar, *Adv. Mater.* **2016**, *28*, 6804–6834; c) S. W. Eaton, M. Lai, N. A. Gibson, A. B. Wong, L. Dou, J. Ma, L.-W. Wang, S. R. Leone, P. Yang, *Proc. Natl. Acad. Sci.*

USA **2016**, *113*, 1993 – 1998; d) J. Xing, X. F. Liu, Q. Zhang, S. T. Ha, Y. W. Yuan, C. Shen, T. C. Sum, Q. Xiong, *Nano Lett.* **2015**, *15*, 4571 – 4577.

[6] a) Y. Zhao, K. Zhu, *Chem. Soc. Rev.* **2016**, *45*, 655 – 689; b) S. Brittman, G. W. P. Adhyaksa, E. C. Garnett, *MRS Commun.* **2015**, *5*, 7 – 26.

[7] a) J. H. Heo, H. J. Han, D. Kim, T. K. Ahn, S. H. Im, *Energy Environ. Sci.* **2015**, *8*, 1602 – 1608; b) A. T. Barrows, A. J. Pearson, C. K. Kwak, A. D. F. Dunbar, A. R. Buckley, D. G. Lidzey, *Energy Environ. Sci.* **2014**, *7*, 2944 – 2950; c) S. Colella, E. Mosconi, P. Fedeli, A. Listorti, F. Gazza, F. Orlandi, P. Ferro, T. Besagni, A. Rizzo, G. Calestani, G. Gigli, F. De Angelis, R. Mosca, *Chem. Mater.* **2013**, *25*, 4613 – 4618.

[8] a) O. Malinkiewicz, C. Roldán-Carmona, A. Soriano, E. Bandiello, L. Camacho, M. K. Nazeeruddin, H. J. Bolink, *Adv. Energy Mater.* **2014**, *4*, 1400345; b) M. Liu, M. B. Johnston, H. J. Snaith, *Nature* **2013**, *501*, 395.

[9] a) C. Xua, S. De, A. M. Balu, M. Ojeda, R. Luque, *Chem. Commun.* **2015**, *51*, 6698 – 6713; b) W. Yuan, T. Friščić, D. Apperley, S. L. James, *Angew. Chem. Int. Ed.* **2010**, *49*, 3916 – 3919; *Angew. Chem.* **2010**, *122*, 4008 – 4011; c) T. Friščić, *Chem. Soc. Rev.* **2012**, *41*, 3493 – 3510; d) S. L. James, C. J. Adams, C. Bolm, D. Braga, P. Collier, T. Friščić, F. Grepioni, K. D. M. Harris, G. Hyett, W. Jones, A. Krebs, J. Mack, L. Maini, A. G. Orpen, I. P. Parkin, W. C. Shearouse, J. W. Steed, D. C. Waddell, *Chem. Soc. Rev.* **2012**, *41*, 413 – 447.

[10] a) X. Ma, G. K. Lim, K. D. M. Harris, D. C. Apperley, P. N. Horton, M. B. Hursthouse, S. L. James, *Cryst. Growth Des.* **2012**, *12*, 5869 – 5872; b) V. André, A. Hardeman, I. Halasz, R. S. Stein, G. J. Jackson, D. G. Reid, M. J. Duer, C. Curfs, M. T. Duarte, T. Friščić, *Angew. Chem. Int. Ed.* **2011**, *50*, 7858 – 7861; *Angew. Chem.* **2011**, *123*, 8004 – 8007.

[11] a) T. Baikie, Y. Fang, J. M. Kadro, M. Schreyer, F. Wei, S. G. Mhaisalkar, M. Graetzel, T. J. White, *J. Mater. Chem. A* **2013**, *1*, 5628 – 5641; b) M. T. Weller, O. J. Weber, P. F. Henry, A. M. Di Pumpo, T. C. Hansen, *Chem. Commun.* **2015**, *51*, 4180 – 4183; c) Q. Han, S.-H. Bae, P. Sun, Y.-T. Hsieh, Y. Yang, Y. S. Rim, H. Zhao, Q. Chen, W. Shi, G. Li, Y. Yang, *Adv. Mater.* **2016**, *28*, 2253 – 2258; d) M. T. Weller, O. J. Weber, J. M. Frost, A. Walsh, *J. Phys. Chem. Lett.* **2015**, *6*, 3209 – 3212; e) N. J. Jeon, J. H. Noh, W. S. Yang, Y. C. Kim, S. Ryu, J. Seo, S. Seok, *Nature* **2015**, *517*, 476 – 480.

[12] A. Dualeh, P. Gao, S. Seok, M. K. Nazeeruddin, M. Grätzel, *Chem. Mater.* **2014**, *26*, 6160 – 6164.

[13] W. Xie, Z. Gao, W.-P. Pan, D. Hunter, A. Singh, R. Vaia, *Chem. Mater.* **2001**, *13*, 2979 – 2990.

[14] M. Szafrański, *Thermochim. Acta* **1997**, *307*, 177 – 183.

[15] M. Szafrański, A. Katrusiak, *Phys. Rev. B* **2000**, *61*, 1026 – 1035.

[16] a) F. Hao, C. C. Stoumpos, Z. Liu, R. P. H. Chang, M. Kanatzidis, *J. Am. Chem. Soc.* **2014**, *136*, 16411 – 16419; b) G. H. Imler, X. Li, B. Xu, G. E. Dobereiner, H.-L. Dai, Y. Rao, B. B. Wayland, *Chem. Commun.* **2015**, *51*, 11290 – 11292; c) A. Lemmerer, D. G. Billing, *CrystEngComm* **2012**, *14*, 1954 – 1966; d) G.-E. Wang, G. Xu, M.-S. Wang, J. Sun, Z.-N. Xu, G.-C. Guo, J.-S. Huanga, *J. Mater. Chem.* **2012**, *22*, 16742 – 16744.

[17] N. De Marco, H. Zhou, Q. Chen, P. Sun, Z. Liu, L. Meng, E.-P. Yao, Y. Liu, A. Schiffer, Y. Yang, *Nano Lett.* **2016**, *16*, 1009 – 1016.

[18] Y. Wang, T. Gould, J. F. Dobson, H. Zhang, H. Yang, X. Yao, H. Zhao, *Phys. Chem. Chem. Phys.* **2014**, *16*, 1424 – 1429.

[19] a) R. Lindblad, D. Bi, B.-W. Park, J. Oscarsson, M. Gorgoi, H. Siegbahn, M. Odelius, E. M. J. Johansson, H. Rensmo, *J. Phys. Chem. Lett.* **2014**, *5*, 648 – 653; b) B. Conings, L. Baeten, C. De Dobbelaere, J. D'Haen, J. Manca, H. G. Boyen, *Adv. Mater.* **2014**, *26*, 2041 – 2046.

[20] B. Wang, K. Y. Wong, S. Yang, T. Chen, *J. Mater. Chem. A* **2016**, *4*, 3806 – 3812.

[21] J. Torrent, V. Barrón in *Encyclopedia of Surface and Colloid Science* (Ed.: P. Somasundaran), Marcel Dekker, New York, **2002**.

[22] V. D'Innocenzo, G. Grancini, M. J. P. Alcocer, A. R. S. Kandada, S. D. Stranks, M. M. Lee, G. Lanzani, H. J. Snaith, A. Petrozza, *Nat. Commun.* **2014**, *5*, 3586.

[23] L. Dimesso, A. Quintilla, Y.-M. Kima, U. Lemmer, W. Jaegermann, *Mater. Sci. Eng. B* **2016**, *204*, 27 – 33.

[24] Y. Li, W. Yan, Y. Li, S. Wang, W. Wang, Z. Bian, L. Xiao, Q. Gong, *Sci. Rep.* **2015**, *5*, 14485.

Received: July 31, 2016
Published online: October 28, 2016

